EEET ECOLOGICAL ENGINEERING & ENVIRONMENTAL TECHNOLOGY

Ecological Engineering & Environmental Technology, 2026, 27(5), 322–340
https://doi.org/10.12912/27197050/220344
ISSN 2719–7050, License CC-BY 4.0

Received: 2026.03.18
Accepted: 2026.04.15
Published: 2026.05.01

High-resolution remote sensing for dominant seagrass species mapping

Agus Aris[1,2*], Supriadi Mashoreng[3], Eymal B. Demmalino[4], Chair Rani[3], Sumarni Hamid Aly[5,6], Nurjannah Nurdin[3,7]

[1] The Environmental Science Study Program Doctoral Program, Hasanuddin University Graduate School
[2] Department of Remote Sensing and Geographic Information Systems, Vocational Faculty, Hasanuddin University, Jl. Perintis Kemerdekaan km.10, Makassar 90245, Indonesia
[3] Department of Marine Science, Faculty of Marine Science & Fisheries, Hasanuddin University, Makassar, 90245, Indonesia
[4] Environmental Science Study Program, Graduate School, Hasanuddin University, Jl. Perintis Kemerdekaan Km 10, Makassar 90245, Indonesia
[5] Department of Environmental Engineering, Engineering Faculty, Hasanuddin University, Jl. Perintis Kemerdekaan Km 10, Makassar 90245, Indonesia
[6] Transportation and Air Quality Research Group, University of Hasanuddin, St. Perintis Kemerdekaan No. KM. 10, South Sulawesi, Makassar 90245, Indonesia
[7] Geospatial Science for Coastal, Marine, and Small Island (GeoSEA) Laboratory, Research and Development Center for Marine, Coast and Small Islands, Hasanuddin University, Makassar 90245, Indonesia
* Corresponding author's email: agus.aris@unhas.ac.id

ABSTRACT

Accurate mapping of dominant seagrass species is an important aspect of supporting ecosystem monitoring and sustainable coastal zone management. This study aimed to integrate high-resolution PlanetScope SuperDove imagery with field observation data to map the spatial distribution of dominant seagrass species around Barrang Lompo Island, Makassar, Indonesia. Three machine learning algorithms, random forest (RF), support vector machine (SVM), and k-nearest neighbor (kNN), were applied and compared to evaluate classification performance. The results showed that the total seagrass coverage reached 52.32 ha, with Thalassia hemprichii identified as the dominant species by the RF and SVM models (covering 20.85 ha and 31.95 ha, respectively), whereas the kNN model identified Cymodocea rotundata as the dominant species. Accuracy evaluation indicated that RF provided the best performance with an overall accuracy of 73% and a kappa coefficient of 0.57, compared to SVM (56%; 0.25) and kNN (60%; 0.36). These findings demonstrate that utilizing high-resolution PlanetScope imagery combined with machine learning approaches is effective for seagrass mapping at the species level in complex shallow waters. The generated distribution maps quantify the extent of dominant seagrass species, providing baseline data for blue carbon estimation, biodiversity assessment, and coastal habitat management.

Keywords: seagrass, high-resolution, planetscope imagery, remote sensing, coastal ecosystems

INTRODUCTION

Seagrass ecosystems play a vital role in maintaining ecological balance, supporting marine biodiversity, and functioning as significant carbon sinks within coastal environments (Nurdin et al., 2022). However, these ecosystems are increasingly under threat due to anthropogenic pressures and the impacts of climate change, including rising sea surface temperatures, sea level rise, and alterations in precipitation patterns (Unsworth et al., 2021). Indonesia, which hosts one of the largest seagrass distributions in the world, these pressures have led to notable degradation in both extent and species composition. Barrang Lompo Island, one of the small islands located in South Sulawesi, harbors an ecologically and economically important seagrass ecosystem that supports

the livelihoods of the local community. Despite its importance, information regarding the spatial distribution and species composition of seagrass in this area remains limited, which are essential for monitoring and management.

A major challenge in managing seagrass ecosystems lies in the limited availability of accurate spatial and temporal data on species distribution, especially in small island environments such as Barrang Lompo. Remote sensing offers a promising approach for mapping and monitoring seagrass ecosystems efficiently over wide and inaccessible areas (McKenzie et al., 2021). However, the effectiveness of this approach depends on proper image classification methods, as well as validation with field data to account for local environmental variability. To address this gap, the present study aims to characterize and map the spatial distribution of dominant seagrass species in Barrang Lompo Island using satellite-based classification techniques. Specifically, this research seeks to identify the dominant seagrass species and their spatial extent by integrating remote sensing data with field observations.

Few seagrass mapping efforts has been conducted in Barrang Lompo using mid-resolution satellite imagery such Landsat 8, Sentinel-2. Such application is useful in large-scale mapping, but its limited in terms of accuracy in capturing the very dynamic habitat features of seagrass meadows (Hamad et al., 2022; Kutser et al., 2020; Lønborg et al., 2022). The use of satellite image classification has become increasingly significant in seagrass mapping due to several advantages. First, satellite imagery enables efficient mapping of wide and often inaccessible coastal areas, reducing the time and cost required for extensive field surveys. Second, satellite sensors such as Sentinel-2,Landsat and PlanetScope provide high temporal resolution, allowing continuous monitoring of seagrass dynamics over time (Traganos et al., 2018). Third, with appropriate classification algorithms, satellite imagery can distinguish seagrass species based on their spectral signatures, facilitating species-level mapping and ecological assessment (Lyons et al., 2020).

Some studies have shown that machine learning can manage nonlinear variations by capturing complex relationships between variables that are difficult to model using traditional linear approaches. For example, algorithms such as support vector machines, neural networks, and random forests can automatically capture nonlinear interactions and threshold effects, thereby improving the predictive power and robustness to noise in multidimensional data (Kyriazos and Poga, 2024) This study aims to produce the first high-resolution dominant seagrass species map on Barrang Lompo Island through the integration of PlanetScope imagery and field data. We hypothesized that the random forest algorithm would provide higher classification accuracy than the support vector machine and k-nearest neighbors. Furthermore, each type of dominant seagrass is assumed to exhibit distinct spectral responses, allowing for the identification of their spatial distribution patterns. Thus, this research can contribute to the detailed identification of dominant seagrass species distribution patterns, supporting the development of the most accurate coastal ecosystem mapping for conservation and management purposes.

MATERIAL AND METHODS

Study area

This research was conducted on Barrang Lompo Island, Spermonde Archipelago, Makassar City, South Sulawesi. The research location was determined based on the results of a preliminary survey, taking into account areas with dense and diverse seagrass ecosystems. Barrang Lompo Island is located at coordinates 5°2′54.640″S, 119°19′45.020″E (Figure 1). The surrounding waters have significant coastal and marine resource potential, including seagrass with an estimated seagrass cover area of more than 50 ha (Nurdin et al., 2022; Nurdin et al., 2023).

Satellite data

The satellite imagery used was SuperDove from PlanetScope, which has 8 bands with a spatial resolution of 3 meters. PlanetScope was chosen because it has a daily temporal resolution, which is crucial for aligning with field survey times and allowing the selection of images with optimal conditions, such as minimal cloud cover and low tide, to maximize mapping accuracy. The satellite imagery used was on April 12, 2025, because it is closest to the survey day. Some of the spectral bands applied in this study include blue

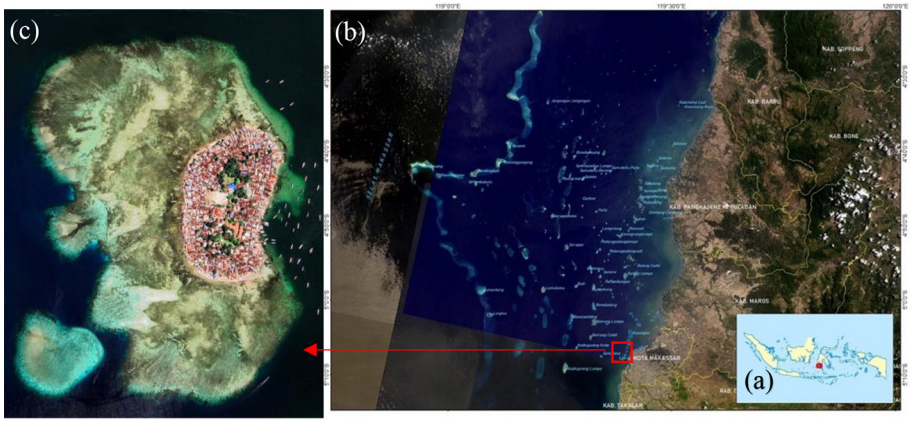

Figure 1. Research location showing: (a) Indonesia with the highlighted study area, (b) the Spermonde Archipelago off the coast of south Sulawesi, (c) Barrang Lompo island as the specific site of investigation

(465–515 nm), green (547–585 nm), red (650–680 nm), and near infrared (845–885 nm).

Field data collection

A field survey was conducted to determine distribution patterns, seagrass ecosystem cover, and species composition. Field data collection was conducted on May 7–8, 2025. Seagrass data collection was conducted using the phototransect method (Sjafrie et al., 2025). A 100-meter transect line was installed perpendicular to the coastline, with a distance of 50 meters between stations. Data collection was carried out using 50 × 50 cm quadrats, placed at 10-meter intervals along the transect. Detailed protocols phototransect measurements are available in the Data Availability Statement. Observation stations were selected based on area characteristics considered to be representative of the entire seagrass area to be surveyed (Nawaz et al., 2025). Each quadrat was documented using a camera equipped with GPS to ensure the location coordinates were recorded accurately. In addition to the transect method, data were also collected randomly in shallow waters, still using the quadrat as the observation unit. This approach aimed to capture variations in seagrass conditions that were not fully represented by the transects (Hamad et al., 2022). The number of sampling points was determined by considering the spatial distribution of observation points and the variation in seagrass habitats so that the ecosystem conditions could be thoroughly represented and the potential for spatial bias minimized (Van Houte-Howes et al., 2004). The data obtained from these field measurements were used as reference points for modeling and validating the results of satellite image classification.

Field data analysis

Identification of seagrass cover and species

The resulting transect photos were then interpreted and analyzed using the Coral Point Count with Excel Extension (CPCe version 4.1) application (Urbina-Barreto et al., 2021; Wang et al., 2024) to obtain the percentage cover of each seagrass species. CPCe is specifically designed to quickly and efficiently calculate coral cover statistically in a specific area. However, this application has also been used to calculate the type and percentage of seagrass cover (Roelfsema et al., 2015; Wicaksono et al., 2023).

Field data alignment with PlanetScope imagery

Field data generalization is necessary to ensure its suitability for remote sensing mapping. In image classification, one pixel is assumed to represent one object, so the field data needs to be adjusted to the pixel size of PlanetScope imagery, which has a spatial resolution of 3 × 3 m. The adjustment of field data to the spatial scale of the imagery was carried out by adopting the method from (Wicaksono et al., 2023). Grids of similar size were used to represent image pixels. Each transect overlapping one grid cell was then used to calculate the average percentage of seagrass cover, so that if there is more than one type of cover in one pixel, the proportion of each type can still be represented

quantitatively. The results of this calculation were then used as training and validation samples for the classification process. The integration scheme for field data into PlanetScope imagery with a resolution of 3 × 3 m is presented in (Figure 2).

Seagrass classification scheme

The classification scheme in this study adopts the approach of (Wicaksono et al., 2023), which is designed to suit the capabilities of PlanetScope satellite data in mapping seagrass ecosystems. Two main indicators are used as the basis for grouping. The first indicator is the distribution between seagrass and non-seagrass, which is considered relevant to describe the distribution in coastal areas. The main classes in this category include seagrass cover condition <25%, seagrass cover 25–50%, seagrass cover 50–75%, and seagrass cover >75% (Figure 3). Each field data point is then classified into one of these categories by considering the most dominant type of substrate cover in the field photos.

The second indicator focuses on variations in the composition of dominant seagrass species. Mapping at the individual species level is difficult due to the limited spatial resolution of the images and the complexity of the seagrass ecosystem, where up to six species can grow in a single pixel. This scheme divides seagrass into four categories: the dominant types *Enhalus acoroides* (Ea), *Thalassia hemprichii* (Th), *Cymodocea rotundata* (Cr), and *Halodule pinifolia* (Hp), which is the dominant class on the island.

Seagrass ecosystem classification

Pra-processing

The initial step in image processing is the separation of land and sea using a masking process using the normalized difference water index (NDWI) method. Next, deep-sea waters are visually masked to focus the study area only on shallow water zones, which are the natural habitat of seagrass. Afterward, sunglint correction and water column correction are applied to the satellite imagery. The sunglint correction method is carried out using a mathematical approach (Nguyen et al., 2021; Song et al., 2020). Water column correction is applied to channels that do not experience glint. A simple water column correction method developed by Lyzenga, known as the depth invariant index (DII), is used to normalize variations in object reflectance due to depth (Wicaksono and Lazuardi, 2018) (Figure 4).

Training data model and validation

After pre-processing, the training point generation and model validation stages were performed randomly. A total of 585 training points and 583 validation points were prepared to map the distribution of seagrass. However, for the classification of cover and dominant seagrass species, filtering was performed to retain only points located within the seagrass area, resulting in 334 training points and 354 model validation points. These samples were converted into polygons in SAGA GIS using Method 4 (Neumann) with a

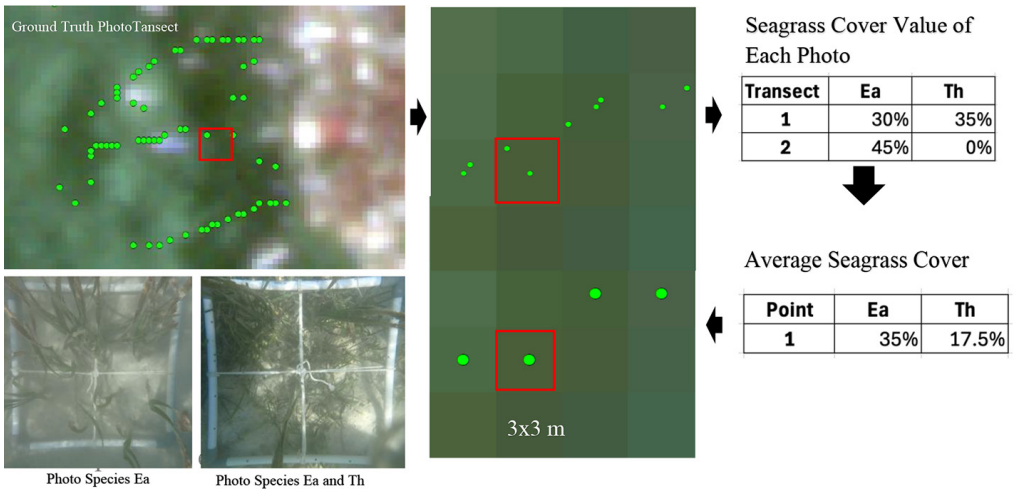

Figure 2. Field data generalized scheme into 3 × 3 m resolution PlanetScope imagery adapted from (Wicaksono et al., 2022). Ground-truth photo transects (top-left) and field photo transcest of seagrass species (bottom-left) were aggregated into PlanetScope pixel grids (center). Seagrass cover values were calculated per transect (top-right) and averaged within a 3 × 3 m grid cell (bottom-right)

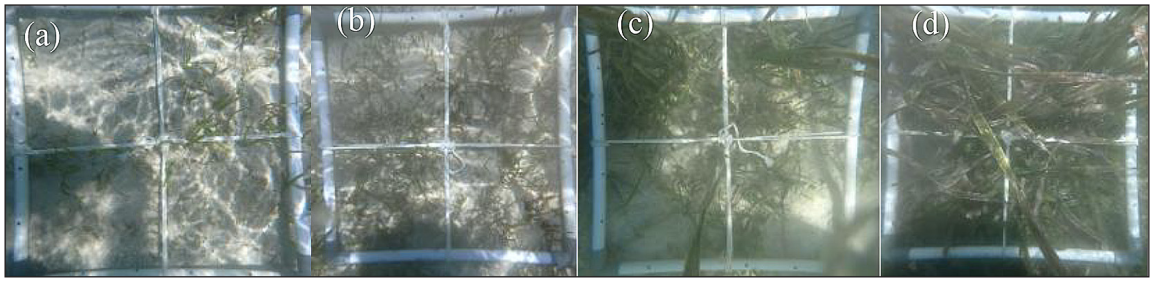

Figure 3. (a) Seagrass cover <25%, (b) seagrass cover 25–50%, (c) seagrass cover 50–75%, (d) seagrass cover >75%

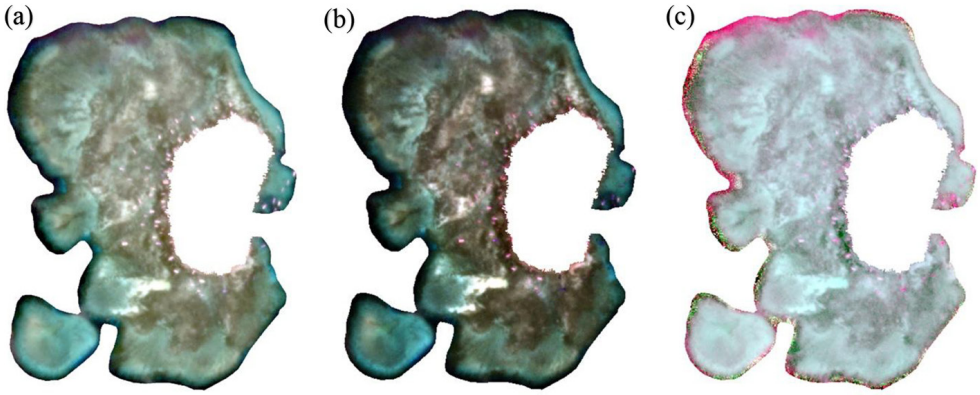

Figure 4. Pre-processing steps applied to satellite imagery: (a) land and deep-sea masking, (b) sun glint removal, and (c) water column correction (depth invariant index)

bandwidth parameter of 0.5. The statistical distribution of spectral reflectance values for each seagrass species across all image bands is shown in Figure 5, which provides insight into the spectral uniqueness of each class and the consistency between the training and validation datasets. Spectral values from image pixels overlapping with the 583 field validation points were analyzed (Figure 5a). To improve classification reliability, a normalization process was performed by removing the 5–10 lowest spectral values that could cause noise or decrease accuracy. The results after normalization are shown in (Figure 5b).

Seagrass segmentation

Mapping seagrass and non-seagrass is the initial stage before distinguishing the dominant seagrass species using a segmentation approach. The segmentation algorithm used is the "Neumann" method using a bandwidth parameter of 2, thus producing homogeneous image objects (Lang et al. 2018). The segmentation results are then integrated with field survey data, which includes seagrass observation points to sample selection accuracy. Training and validation polygons are determined through a segmentation process with a bandwidth of 0.5 carried out using SAGA GIS version 9.11.1 software. Training data for classification is developed separately for each type of seagrass to distinguish variations in spectral characteristics. Based on this training data, classification is carried out using two approaches, namely combining object segmentation processes and machine learning-based classification (supervised classification).

Pixel-based classification

This study employed three machine learning algorithms: Random forest (RF), support vector machine (SVM), and k-nearest neighbor (kNN), using SAGA GIS software (Figure 7). The RF algorithm constructs an ensemble of decision trees, each trained on a subset of data and random inputs. The final result is obtained through a majority vote from all the trees. This approach makes the model more effective and stable in prediction and reduces overfitting (Ha et al., 2020; Price et al., 2022). The main principle of RF is to determine the class based on Decisions; this model was run in SAGA GIS using 1.000 trees to train the model, a maximum tree depth of 10, a minimum number of samples of 2, and a maximum of

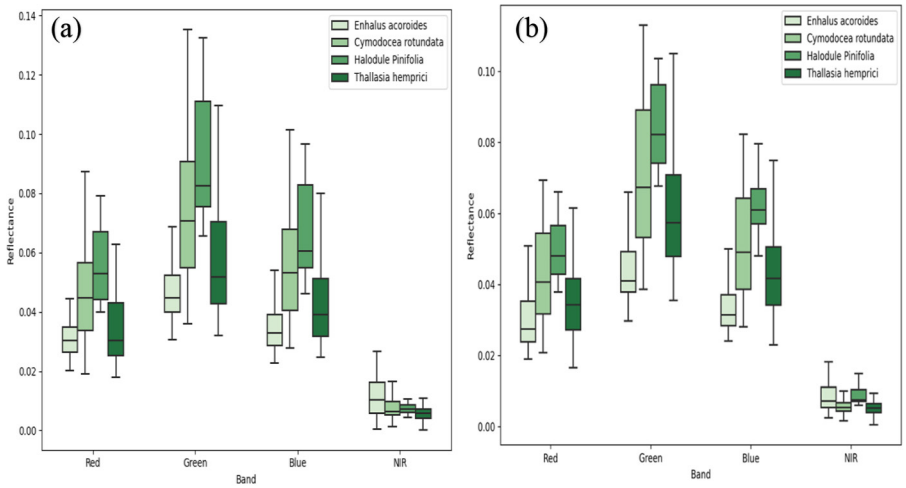

Figure 5. Boxplot of spectral values for dominant seagrass types: (a) model points and (b) validation points

10 categories. The 1SE rule and truncate pruned trees options were enabled to control model complexity. The SVM implementation uses the C-Support Vector Classification (C-SVC) variant with a radial basis function (RBF) kernel (Kaul and Raina, 2022). Parameters used include a C value of 1 and a gamma value of 5. Other parameters such as degree (3), coef0 (0), and epsilon (0.001) use the default settings from SAGA GIS. The kNN algorithm is a commonly used machine learning technique for classification and regression purposes (Guo et al., 2018). In this study, the kNN parameter configuration uses the default values, with the number of neighbors set to 3 and the brute-force nearest neighbor search method.

The training and validation points for the kNN and SVM models followed the same methodology as those applied to the RF model to ensure consistent comparisons between the methods. The classification map was validated using a 5m resolution single pixel set obtained from a field survey. A total of 354 pixels were extracted from the boundaries of the classified objects using a sampling method. The use of polygons with a large number of pixels generally helps with robust training data. However, in this study, the approach in the validation stage, selecting a single pixel, was used to increase the objectivity of the validation process, so that classification errors could be detected effectively.

Accuracy assessment

To evaluate the classification results, a confusion matrix was constructed for each machine learning algorithm using the validation dataset. The accuracy assessment approach included overall accuracy (OA), producer accuracy (PA), user accuracy (UA), and Cohen's kappa coefficient (Congalton et al., 2008). The error matrix method used in this study follows the following formula:

$$K = \frac{N\sum_{i=1}^{r} X_{ii} - \sum_{i=1}^{r}(X_{i+} \cdot X_{+i})}{N^2 - \sum_{i=1}^{r}(X_{i+} \cdot X_{+i})} \quad (1)$$

where: N is the total number of samples, xii is the diagonal value of the matrix (correctly classified samples), $xi+$ is the total rows for a class, $x+i$ is the total columns for a class, k is the number of classes

Spectral characterization of seagrass

Spectral characterization was conducted through field measurements using a spectroradiometer and PlanetScope satellite imagery to analyze the reflectance characteristics of the various seagrass species. Field spectral measurements were conducted using a portable Lambda NIR spectroradiometer, covering the 350–1000 nm spectral range, under clear weather and calm waters (Figure 6) (Nurdin et al. 2016). Before and during the measurements, the instrument was calibrated using a Spectral on white panel to ensure radiometric accuracy. Each spectral measurement was repeated at the nadir position, approximately 2 cm above the seagrass canopy. Detailed protocols spectral measurements are available in the Data Availability Statement. The obtained spectral data were normalized, denoised, and graphically visualized. The final

Figure 6. (a) Field Lambda NIR spectroradiometer covering a spectral range of 350–1000 nm, (b) sensor cable for the white reference and the object, (c) white reference correction, (d) reflectance measurement of seagrass

dataset included 21 spectral features for each species. Distinctive spectral features in the visible and near-infrared regions were identified, and dendrogram analysis was performed using Google Colab to assess the level of similarity and as validation data.

PlanetScope imagery, which has four spectral resolutions (Blue, Green, Red, and Near-Infrared), was first geometrically aligned with the field data. The area corresponding to the field measurement location was extracted from each pixel and converted into spectral values. The reflectance profiles generated from PlanetScope satellite imagery were analyzed using Google Colab (Python 3.12) with the libraries pandas (2.2.2), numpy (2.0.2), matplotlib (3.10.0), seaborn (0.13.2), scipy (1.16.3), and openpyxl (3.1.5), used with the dendrogram method to assess the level of spectral similarity of each seagrass species (Figure 7). The results of this analysis serve as validation material to evaluate the accuracy of PlanetScope satellite imagery.

Seagrass spatial distribution

By using the results of random forest classification, the distribution patterns of seagrass were identified through a buffer analysis approach. This method uses the coastline as a reference to generate buffer zones with 3 classes: <50 m, 50–100m, and >100 m. This process is used to determine the tendency of seagrass distribution in relation to distance from the coastline (Figure 8).

RESULTS

Seagrass identification and mapping

Based on field survey results, six seagrass species were identified in the waters of Barrang Lompo Island: *Syringodium isoetifolium* (Si), *Cymodocea rotundata* (Cr), *Halophila ovalis* (Ho), *Enhalus acoroides* (Ea), *Halodule pinifolia* (Hp), and *Thalassia hemprichii* (Th). These results are consistent with those of previous studies conducted at the same location (Mashoreng et al. 2021; Nurdin et al. 2022). The distribution of seagrasses in these waters shows significant variations among species. *Thalassia hemprichii* appeared to dominate almost the entire observation path in the study. In contrast, Halophila ovalis has a very limited distribution and is only found in a few locations with sparse cover.

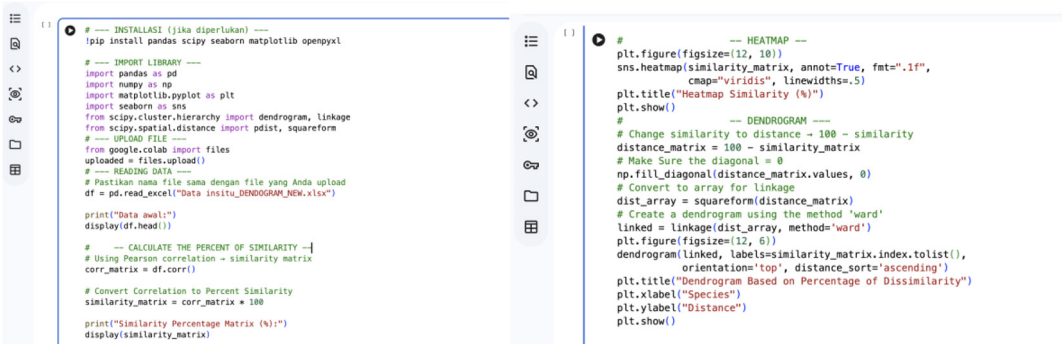

```
# ~~~ INSTALLASI (jika diperlukan) ~~~
!pip install pandas scipy seaborn matplotlib openpyxl

# ~~~ IMPORT LIBRARY ~~~
import pandas as pd
import numpy as np
import matplotlib.pyplot as plt
import seaborn as sns
from scipy.cluster.hierarchy import dendrogram, linkage
from scipy.spatial.distance import pdist, squareform
# ~~~ UPLOAD FILE ~~~
from google.colab import files
uploaded = files.upload()
# ~~~ READING DATA ~~~
# Pastikan nama file sama dengan file yang Anda upload
df = pd.read_excel("Data insitu_DENDOGRAM_NEW.xlsx")

print("Data awal:")
display(df.head())

#    ~~ CALCULATE THE PERCENT OF SIMILARITY ~~
# Using Pearson correlation → similarity matrix
corr_matrix = df.corr()

# Convert Correlation to Percent Similarity
similarity_matrix = corr_matrix * 100

print("Similarity Percentage Matrix (%):")
display(similarity_matrix)
```

```
#                    ~~ HEATMAP ~~
plt.figure(figsize=(12, 10))
sns.heatmap(similarity_matrix, annot=True, fmt=".1f",
            cmap="viridis", linewidths=.5)
plt.title("Heatmap Similarity (%)")
plt.show()
#                    ~~ DENDROGRAM ~~~
# Change similarity to distance → 100 - similarity
distance_matrix = 100 - similarity_matrix
# Make Sure the diagonal = 0
np.fill_diagonal(distance_matrix.values, 0)
# Convert to array for linkage
dist_array = squareform(distance_matrix)
# Create a dendrogram using the method 'ward'
linked = linkage(dist_array, method='ward')
plt.figure(figsize=(12, 6))
dendrogram(linked, labels=similarity_matrix.index.tolist(),
           orientation='top', distance_sort='ascending')
plt.title("Dendrogram Based on Percentage of Dissimilarity")
plt.xlabel("Species")
plt.ylabel("Distance")
plt.show()
```

Figure 7. Python script used to generate the similarity matrix, heatmap, and dendrogram in seagrass spectral analysis

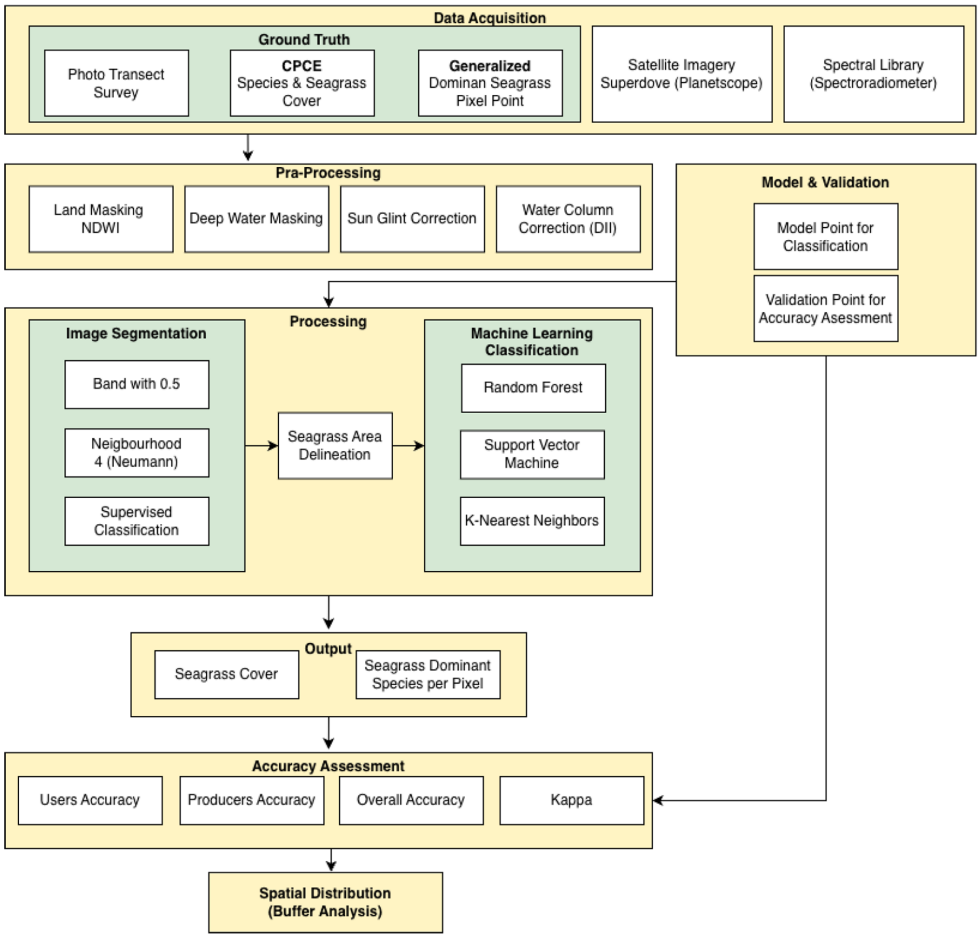

Figure 8. Workflow consists of six main stages, namely: data acquisition, pre-processing, design point of model and validation, processing, accuracy testing in seagrass mapping approaches based on machine learning, and finally buffer analysis to identify the spatial distribution patterns of seagrass

Seagrass and non-seagrass segmentation

In the first stage, mapping successfully distinguished seagrass and non-seagrass areas. Of the 13,930 segments generated, 4.770 were identified as seagrass (Figure 9a). This seagrass and non-seagrass distribution map was then used as the study boundary for the next classification, namely mapping seagrass cover and dominant seagrass species. The use of this masking is crucial to minimize interference from classes other than seagrass and focus the analysis on seagrass areas (Figure 9b). With this approach, the accuracy of identifying dominant seagrass species is expected to improve in the future.

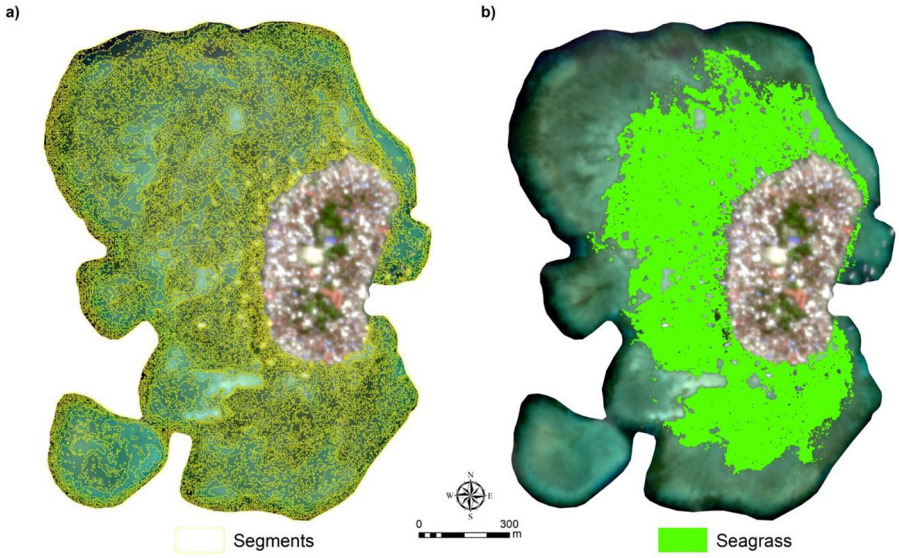

Figure 9. Segmentation results of seagrass and non-segrass: (a) map showing segmented image objects in shallow water, (b) seagrass distribution map highlighting identified seagrass areas

Seagrass percent cover classification

In this study, three machine learning algorithms were compared to map the distribution of seagrass on Barrang Lompo Island. Figure 10 shows the spatial distribution of seagrass cover based on the cover density generated by the three classification algorithms: RF, SVM, and kNN. All three methods were able to map seagrass cover in the waters of Barrang Lompo Island, with varying seagrass cover areas. Table 1. However, based on the accuracy assessment, the RF method performed the best, with a score of 75.4%.

Based on the results of the RF classification (Figure 10a), seagrass cover can be clearly distinguished among the classes of <25%, 25–50%, 50–75%, and >75%. This classification shows that the largest distribution of seagrass cover falls within the 25–50% class, followed by the <25% class. The SVM method (Figure 10b) tends to group large areas and generalize pixels, as seen in the 50–75% and >75% classes, which are often found in the southern part of Barrang Lompo Island. The SVM classification is heavily dominant in the 50–75% cover class, while the 25–50% class only covers a very limited area, around 1.2%. Meanwhile, the k-nearest neighbor (kNN) classification (Figure 10c) displays a scattered and uneven distribution pattern. This method shows that its classification results fall between those of Random Forest and SVM. Although it provides a fairly large area in the 50–75% cover class, kNN also allocates a significant area to the <25% and 25–50% classes.

Seagrass species-level classification

The classification map of dominant seagrass species generated by machine learning methods shows that only four out of the six seagrass species identified in Barrang Lompo were successfully classified. The classification results of

Table 1. Areal extent of seagrass cover classes (Ha) derived from three classification algorithms: Random forest (RF), support vector machine (SVM), and k-nearest neighbors (KNN)

Seagrass cover	Area (ha)		
	RF	SVM	KNN
Seagrass cover <25%	13.24	15.86	11.26
Seagrass cover 25–50%	23.13	0.65	13.33
Seagrass cover 50–75%	10.73	28.45	22.03
Seagrass cover >75%	5.22	7.36	5.71
Total	52.32	52.32	52.32

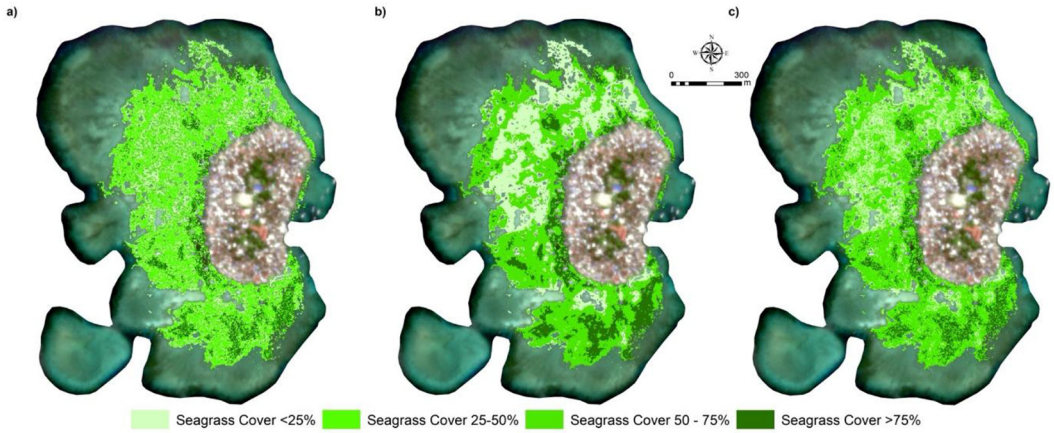

Figure 10. Spatial distribution of seagrass cover derived from three machine learning classification algorithms: (a) Random forest (RF), (b) support vector machine (SVM), (c) k-nearest neighbors (KNN)

the RF algorithm indicate that two main species dominate, namely Thalassia hemprichii and Cymodocea rotundata. Other species, such as Enhalus acoroides, were also successfully detected with a coverage of around 12%, while Halodule pinifolia accounted for only 8.6%. This differs from the results of the SVM classification, which identified only three seagrass species. However, this method also showed a similar dominance by the two seagrass species, Thalassia hemprichii and Cymodocea rotundata. Meanwhile, the kNN method showed a similar classification pattern, successfully identifying four dominant seagrass species (Table 2). The spatial distribution maps of the dominant seagrass species throughout Barrang Lompo Island, produced by the RF, SVM, and k-nearest neighbor (kNN) algorithms, are presented in Figure 11.

Based on Figure 11a, the results of the RF classification showed that *Thalassia hemprichii* (yellow) and *Cymodocea rotundata* (blue) emerged as the most widespread species, particularly in areas with relatively high cover density. *Enhalus acoroides* (red) was consistently concentrated in shallow water zones near the coast, particularly in the western and southern coastal areas of Barrang Lompo Island. In contrast, the SVM classification method (Figure 11b) produced a wider and more homogeneous distribution area, with a strong emphasis on *T. hemprichii* and *C. rotundata*, indicating a tendency to simplify spectral variability. Meanwhile, the KNN classification method (Figure 11c) produced different results between the two methods. This method was still able to represent the diversity of dominant seagrass species but showed uneven distribution patterns, which was likely caused by its sensitivity to local spectral similarities.

Accuracy assessment seagrass classification

Based on the accuracy test, the classification results for seagrass and non-seagrass species showed an accuracy rate of 83.64% (Table 3), indicating that the classification method used was effective for mapping seagrass distribution. The error matrix shows that of the 403 seagrass validation points, 354 points were correctly identified as

Table 2. Estimated seagrass cover area (ha) based on dominant species using three classification algorithms: Random forest (RF), support vector machine (SVM), and k-nearest neighbors (kNN)

Species	Area (ha)		
	RF	SVM	kNN
Cymodocea rotundata	20.71	19.40	25.23
Enhalus acoroides	6.26	0.96	3.13
Halodule Pinifolia	4.49	-	1.61
Thallasia hemprici	20.85	31.95	22.33
Total	52.32	52.32	52.32

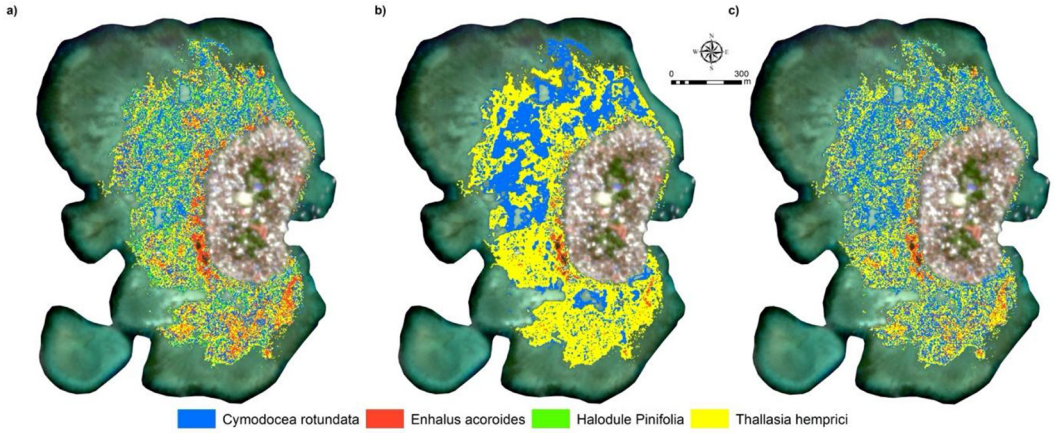

Figure 11. Spatial distribution of dominant seagrass species derived from three classification algorithms: (a) Random forest (RF), (b) Support vector machine (SVM), and (c) k-nearest neighbors (KNN). The classified species included *Cymodocea rotundata* (blue), *Enhalus acoroides* (red), *Halodule pinifolia* (green), and *Thalassia hemprichii* (yellow)

seagrass. Meanwhile, 172 of the 180 non-seagrass pixels were correctly classified. The user accuracy values for seagrass and non-seagrass classes reached 87.84% and 95.56%, respectively, while the producer accuracy values were 97.79% for seagrass and 77.83% for non-seagrass. The high accuracy value in identifying seagrass classes indicates that this method can recognize seagrass characteristics well; therefore, it can be used as a reference for mapping dominant seagrass species.

This study demonstrated the accuracy level using an error matrix to classify dominant seagrass species within the seagrass cover. Based on the application of three machine learning algorithms, RF performed best compared to other methods. This algorithm achieved an overall accuracy of 73% and a kappa coefficient of 0.57 (Table 4). Specifically, the RF method demonstrated the best accuracy in classifying *Thalassia hemprichii* and *Enhalus acoroides*, with producer accuracy (PA) values of 74.2% and 69.2%, respectively, and user accuracy (UA) values of 80% and 73.8%, respectively. Conversely, *Halodule pinifolia* showed the lowest accuracy level among all the methods tested. The kNN classification method produced intermediate performance, with an overall accuracy of 0.60 and a kappa coefficient of 0.36. This method provided relatively good results in classifying *Cymodocea rotundata*, but its performance was less than optimal for *Halodule pinifolia* and *Enhalus acoroides*.

Seagrass spectral reflectance

The results of spectroradiometer measurements (Figure 12a) show the spectral profiles of four dominant seagrass species, which exhibit distinct reflectance characteristics in the 400–900 nm wavelength range. Seagrass Cr exhibits the typical spectral characteristics of healthy seagrass, characterized by low reflectance in the visible spectrum from 400–700 nm, followed by a sharp increase at the red edge around 700 nm, and reaching a peak reflectance of 16% in the near-infrared (NIR: 700–900 nm). This pattern is related to the internal structure of the leaves, which can reflect infrared radiation. Similar patterns are also observed in other species, where reflectance levels are consistently low across visible

Table 3. Overal accuracy seagrass area mapping

Class	Seagrass	Non-seagrass	Total	UA
Seagrass	354	49	403	87.84
Non-seagrass	8	172	180	95.56
Total	362	221		
PA	97.79	77.83		
OA	83.64			

Table 4. Overall accuracy assessment and kappa of seagrass classification using RF, SVM, and kNN, showing Overall accuracy and Kappa coefficient

ML classification method	Overall	Kappa
RF	73%	0.57
SVM	56%	0.25
KNN	60%	0.36

wavelengths, but slightly increase at green wavelengths and peak in the NIR region.

Based on the results of the extraction of spectral values of seagrass species from PlanetScope images (Figure 12b), the four seagrass species exhibited similar spectral reflectance patterns but differing spectral values in the 400–900 nm range. The spectral reflectance of seagrasses exhibits distinct peaks at green and red edge wavelengths. The Hp seagrass species had the highest spectral value, followed by the Cr species. The lowest spectral value at a wavelength of 500–600 nm corresponds to the Ea species. The spectral reflectance patterns of seagrass species using different approaches have similar spectral reflectance patterns but differ in the strength of the reflectance values. In particular, at NIR wavelengths, the spectroradiometer results were higher than those from the PlanetScope satellite image extraction. This is because the Planetscope is still affected by the water column, while using a spectroradiometer, the objects measured are around 2 cm.

DISCUSSION

Machine learning-based seagrass mapping

The classification results from RF, SVM, and kNN show that the seagrass community is dominated by Thalassia hemprichii and Cymodocea rotundata, with nearly equal distribution. This pattern aligns with previous studies in the Spermonde area, which consistently showed *Thalassia hemprichii* as the dominant seagrass species in shallow waters with relatively stable substrate conditions (Nurdin et al., 2022). In contrast, *Enhalus acoroides* and *Halodule pinifolia* had smaller distribution areas. This limited distribution is related to the ecological characteristics of each species, particularly *E. acoroides*, which generally grows locally in certain areas, such as the study location, which is only found along the coastline. In contrast, *H. pinifolia* tends to form scattered and uneven cover.

Overall, the classification results for seagrass and non-seagrass classes showed an overall accuracy (OA) of 83.64%. This accuracy is significantly higher than that typically obtained from medium-resolution sensors, such as Landsat or Sentinel, thus confirming the superiority of PlanetScope satellite imagery in optically mapping seagrass ecosystems in shallow waters. Of the three algorithms tested, RF produced the highest accuracy of 73%, surpassing SVM at 56% and kNN at 60%. This excellent RF performance is in line with the algorithm's characteristics of constructing an ensemble of decision trees from random combinations of predictor variables, making it more robust to spectral variation. This finding is consistent with previous research showing that RF is highly effective for mapping complex benthic habitats (Meister and Qu, 2024). Although the SVM algorithm is widely used in image classification, the results of this study indicate that it has considerable difficulty generalizing when classes represent only a small portion of the total pixel distribution of the image. This condition resulted in an underestimation of Enhalus acoroides and a failure to detect Halodule pinifolia. Meanwhile, the kNN algorithm produced a moderate level of accuracy. The kNN

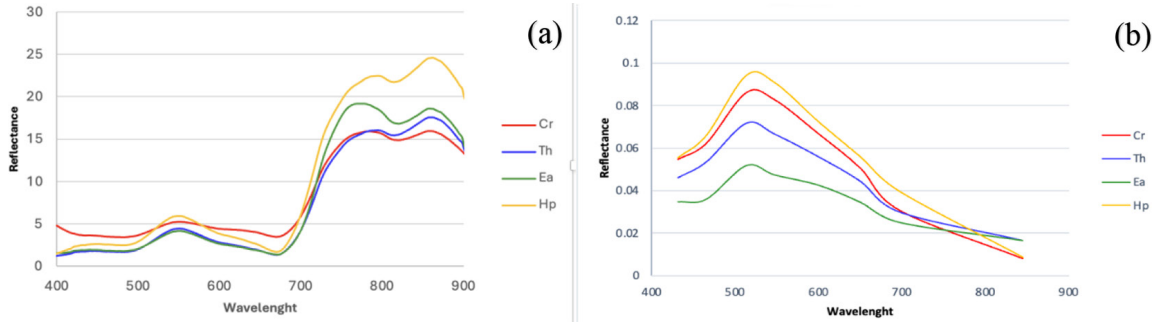

Figure 12. Spectral reflectance of *Cymodocea rotundata* (Cr), *Enhalus acoroides* (Ea), *Thalassia hemprichii* (Th), and *Halodule pinifolia* (Hp) derived from a spectroradiometer

performance is consistent with previous literature findings, particularly for coastal habitat classification applications with high spectral complexity (Marcello and Eugenio, 2022).

For all classification results, the accuracy at the dominant seagrass species level was significantly affected by the spectral overlap between seagrass species. This challenge was most evident in *Halodule pinifolia* and Cymodocea, where the reflectance curves of both species showed very little difference in the visible to near-infrared spectral region. A similar phenomenon has been described in previous studies, which emphasized that tropical seagrass species generally have similar spectral characteristics and are difficult to distinguish using multispectral satellite imagery (Wicaksono, 2023).

Accuracy evaluation to demonstrate model performance is determined not only by the overall accuracy value but also by the producer and user accuracy in each class. The relatively small difference between the producer accuracy (PA) and user accuracy (UA) in most classes (Figure 13) indicates that the developed model has a good level of stability. However, the large PA–UA difference in the E. acoroides class in the SVM classification, which reached 65.2%, reflects inconsistencies with the reference data. However, the RF method showed almost all small differences between PA and UA accuracy, where the results of the study clearly showed that this method is the best for mapping dominant seagrass species. The findings of this study emphasize the importance of a more representative training data collection strategy, particularly for species with limited distribution areas.

Seagrass species spatial distribution patterns

The zonation analysis of the dominant seagrass species on Barrang Lompo Island clearly correlated with the distance from the shoreline. The analysis revealed that most *Cymodocea rotundata* (15.42 ha) and *Thalassia hemprichii* (15.31 ha) cover was concentrated in areas more than 100 m from the shoreline. In contrast, the nearshore zones, that is, <50 m and 50–100 m, contributed only a relatively small portion to the total seagrass area. A similar pattern was also observed for *Halodule pinifolia*, which tended to grow in zones farther from the shoreline (Figure 14). Unlike other species, *Enhalus acoroides*, although found in all distance zones, remained the most abundant in the outermost zone. However, this species still showed a dominant contribution to the nearshore zone, reflecting its adaptability to varying coastal environmental conditions.

Based on Figure 15a the observed distribution of seagrasses aligns with the ecological characteristics of each species. *Thalassia hemprichii*, with its thick leaves and strong root system, tends to dominate stable and minimally disturbed habitats (Mishra and Apte, 2020). Meanwhile, *Cymodocea rotundata* is found on fine sand substrates and calmer waters and is often found in zones farther from the shoreline. Enhalus acoroides exhibits a wide ecological tolerance range, where its sturdy roots and long leaves allow it to survive in nearshore areas, where anthropogenic activity is present, while growing optimally in deeper, clearer waters. Conversely, *Halodule pinifolia*, a thin-leaved species, often colonizes disturbed substrates, but its spectral reflectance values are almost similar

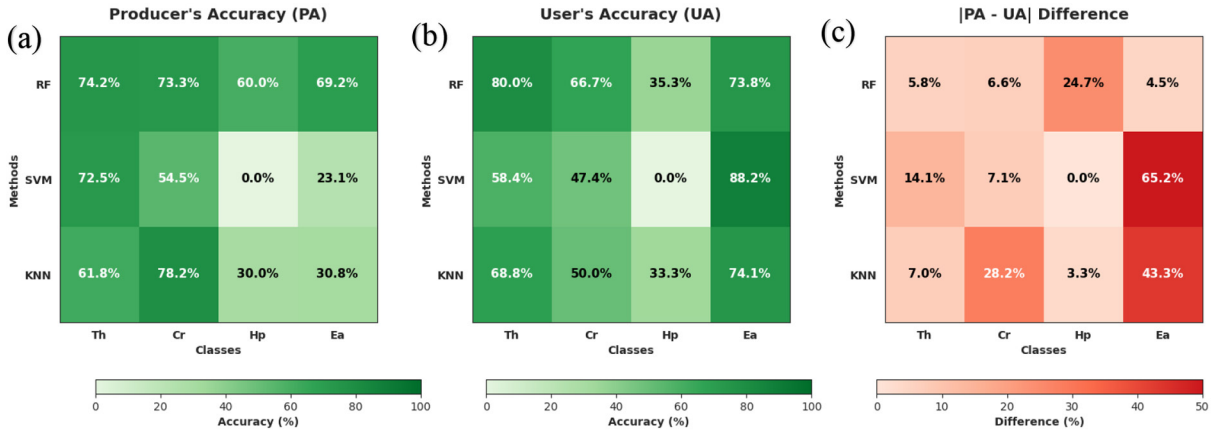

Figure 13. Heatmap: (a) producer accuracy, (b) user's accuracy, c) PA-UA difference

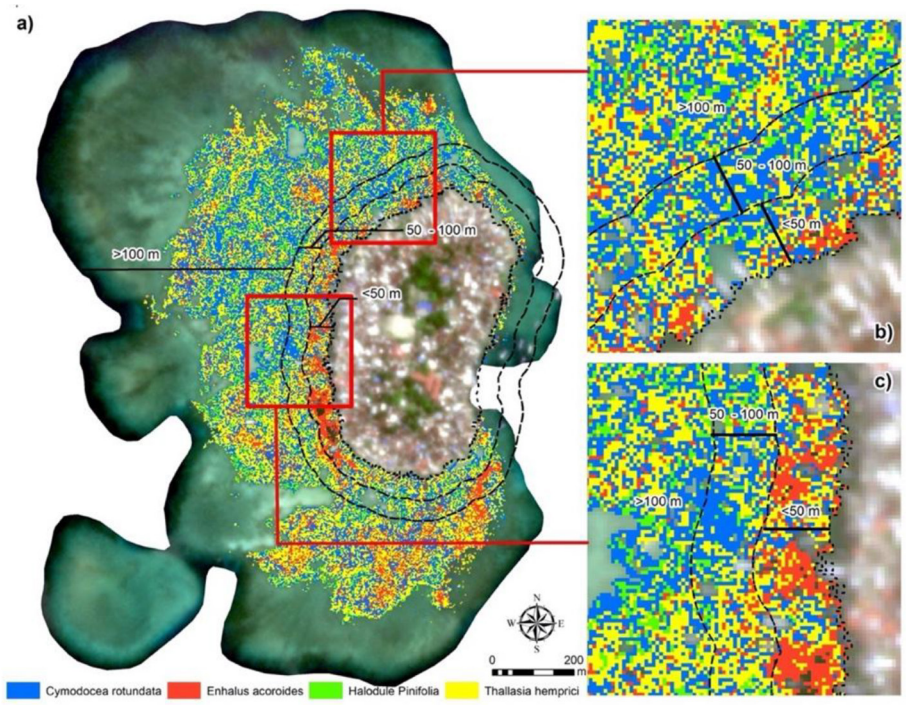

Figure 14. Random forest-based distribution map of seagrass species showing zonation based on distance from the coastline

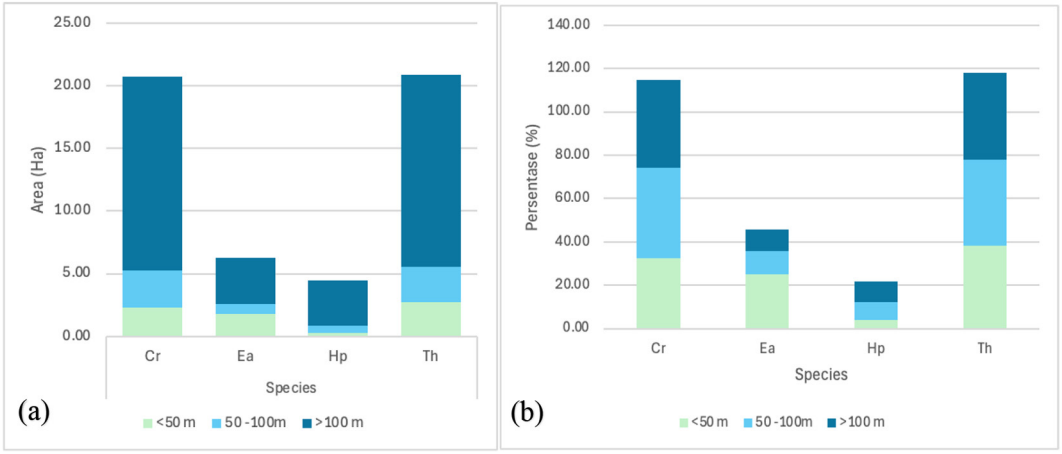

Figure 15. Distribution of seagrass area based on distance from the shoreline (a), proportion of seagrass species by distance zone (%) (b)

to those of other species, making it susceptible to misclassification. However, its small size and limited distribution make this species difficult to detect at a 3 × 3 m pixel scale, especially when mixed with other, more dominant species.

Based on RF classification followed by buffer analysis, the patterns generated in this study reflect the ecological zoning commonly found in tropical seagrass meadows across various regions. Areas closer to the shoreline generally experience higher levels of sediment suspension owing to the influence of stronger waves, resulting in decreased water clarity and limited seagrass growth. Conversely, zones >100 m away (Figure 15b) are characterized by clearer waters and lower sediment pressure, providing a more favorable environment for competitive species, particularly *Thalassia hemprichii* and *Cymodocea rotundata*, to thrive and dominate (Gole et al., 2023). However, the zonation identified in this study has limitations, namely that it is still correlational and cannot be interpreted as a cause

and effect relationship. Therefore, future research should integrate more comprehensive approaches, such as habitat suitability modeling or multivariate analysis, to examine in more detail the role of environmental factors, including water depth, turbidity levels, current dynamics, and substrate characteristics, on seagrass species distribution, as recommended by Kuhwald et al. (2022).

Seagrass species level classification challenges

Classifying seagrass species using optical satellite imagery remains a challenge, as has been widely discussed in previous studies (Hossain et al., 2015; Pittman et al., 2021). The main challenges are related to two key factors: the effects of the water column, which modify the reflectance signal, and the high similarity in spectral patterns between seagrass species and between seagrasses and other benthic substrates, such as sand, macroalgae, organic debris, and epiphytes (Hedley et al., 2017). In the tropical Indo-Pacific region, conditions are increasingly complex owing to the overlapping species diversity and canopy structure of seagrasses at relatively small spatial scales. Consequently, the presence of mixtures of several species within a single pixel is difficult to avoid. At this research site, a single 50 × 50 cm observation plot often contained more than one seagrass species, making separation based on spectral characteristics increasingly complex. This research limitation is reinforced by the fact that multispectral sensors are not yet sensitive enough to distinguish subtle spectral absorption between seagrass species (Wicaksono and Kamal, 2017; Wicaksono et al., 2019a).

The spectral value patterns of the four dominant seagrass species from the two approaches have similar reflectance patterns, but the reflectance values show relatively subtle differences. This indicates sufficient consistency to be utilized in a machine learning-based classification process. This finding is in line with research results (Durako, 2007), which stated that differences in spectral value characteristics between seagrass species appear at green wavelengths (500–600 nm), red-edge (700–750 nm), and near-infrared (700–850 nm). These differences are closely related to variations in the pigment content and leaf anatomical function of each species. Furthermore, (Fyfe, 2004; Hwang et al., 2019) emphasized that leaf pigment concentration, internal anatomical structure, and the presence of epibiont organisms play a significant role in determining the ability of seagrass leaves to reflect light. These factors collectively influence the variations in leaf surface reflectance observed in the spectral measurements. Although these spectral differences between species are relatively small, these nuances still provide important information for classification algorithms to improve class separation. However, spectral overlap remains a major limitation of species-level classification.

Spectral-based clustering analysis of seagrass species

Spectral measurement analysis, obtained from in situ spectrometers and planetscope satellite imagery, plays an important role in determining the most appropriate spectral resolution, selecting the appropriate classification scheme, and designing remote sensing image analysis procedures for seagrass species mapping (Wicaksono et al., 2019b). The reflectance characteristics of tropical seagrass species and their implications for mapping using multispectral satellite imagery have also been widely studied in previous research (Wicaksono et al., 2019). In this study, the input data used in the clustering analysis were the spectral reflectance values for each dominant seagrass species at various wavelengths. The results of the wavelength-based clustering analysis are presented in Figure 16 and 17, which illustrate the level of spectral similarity and separation between the seagrass species.

Based on the results of spectral clustering of in situ measurement data using a spectroradiometer (Figure 15), two groups were formed with compositions different from those found in the PlanetScope data analysis. In the spectroradiometer data, Cluster 1 consists of *Cymodocea rotundata* (Cr), *Enhalus acoroides* (Ea), and *Thalassia hemprichii* (Th), with an average similarity of 59.0%, while Cluster 2 is only filled by *Halodule pinifolia* (Hp). Within Cluster 1, the highest spectral similarity was found between *E. acoroides* and *T. hemprichii* at 69.3%, then between *C. rotundata–T. hemprichii* (57.4%) and *C. rotundata–E. acoroides* (50.4%). This pattern shows that although all three species are in a single cluster, there is a clear gradient in spectral proximity, with *E. acoroides* and *T. hemprichii* being the most similar pair. In contrast, the PlanetScope data-based analysis (Figure 16) shows a more patterned clustering pattern with

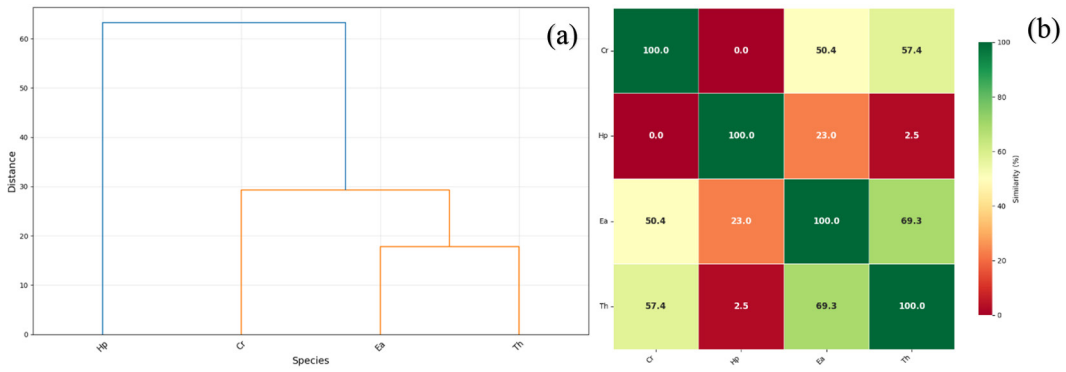

Figure 16. Dendrogram of spectral value similarity for seagrass species (a), heatmap of percentage similarity among seagrass species based on spectroradiometer measurements (b)

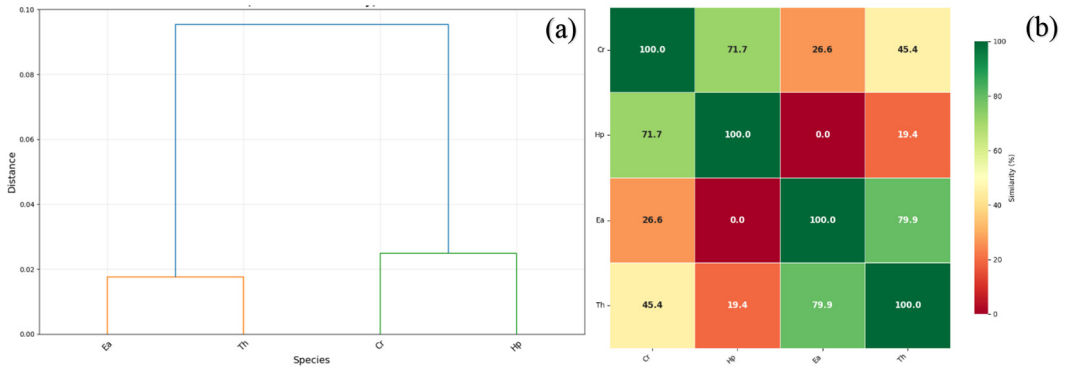

Figure 17. Dendrogram of spectral value similarity for seagrass species (a), heatmap of percentage similarity among seagrass species based on spectral values from PlanetScope imagery (b)

two clearly separated clusters. Cluster 1 consists of *E. acoroides* and *T. hemprichii*, which show a very high level of spectral similarity of 79.9%, while Cluster 2 consists of *C. rotundata* and *H. pinifolia* with a similarity of 71.7%. These results confirm the consistency of spectral closeness between *E. acoroides* and *T. hemprichii* on both measurement platforms, although the similarity level was higher in the satellite data.

The differences in cluster structure between the spectroradiometer and PlanetScope data were likely influenced by several factors, including differences in the spectral resolution of the two sensors, atmospheric influences on satellite data, and the influence of the water column on satellite imagery. The finding that *H. pinifolia* formed a separate cluster in the in situ data but joined *C. rotundata* in the PlanetScope data reflects the complexity of interpreting remote sensing data for seagrass species identification in this region. The high spectral similarity between *E. acoroides* and *T. hemprichii* on both platforms, 69.3% in the spectroradiometer and 79.9% in PlanetScope, indicates strong similarities in bio-optical characteristics, which may be related to taxonomic closeness or morphological and physiological similarities between the two species. This pattern is consistent with the findings of Hartoni et al. (2022), who reported a high spectral similarity between the two seagrass species (Figure 17).

CONCLUSIONS

This study demonstrates that the use of PlanetScope imagery combined with machine learning approaches can produce fairly accurate maps of dominant seagrass ecosystem types. Field surveys identified six seagrass species, of which four dominant species *Thalassia hemprichii*, *Cymodocea rotundata*, *Enhalus acoroides*, and *Halodule pinifolia* were successfully mapped after data generalization. These in situ observations were

crucial for training and validating the classification model, thereby increasing the confidence in mapping results. Among the three machine learning algorithms applied, RF consistently showed the highest performance, with an overall accuracy of 83.6% for classifying seagrass and non-seagrass, and a 73% accuracy for mapping dominant seagrass species. This illustrates RF's ability to handle the high spectral variability in the complex shallow water environment. Support vector machine had limitations in detecting species with small or fragmented distributions, while kNN provided moderate accuracy but less stable results.

Spatial analysis revealed that the distribution patterns of *Thalassia hemprichii* and *Cymodocea rotundata* were concentrated in zones >100 m from the shoreline, characterized by deeper and clearer waters with lower sediment disturbance. On the other hand, *Enhalus acoroides* maintained significant coverage, but its dominant percentage was within <50 m of the coast. Spectral analysis using a field spectroradiometer and PlanetScope imagery showed subtle yet consistent differences in reflectance between species, especially in the visible spectrum, although there was some spectral overlap between Ea and Th species. Further clustering processes identified two main spectral groups (Ea + Th) and (Cr + Hp), providing insights to refine classification methods in future studies.

Overall, these findings indicate that mapping dominant seagrass types using multispectral satellite data is highly feasible, offering reliable baseline information for biodiversity monitoring, blue carbon estimation, and sustainable coastal management. This study also establishes a methodological framework for high-resolution seagrass mapping in similar shallow marine ecosystems in the future.

REFERENCES

1. Congalton, R. G., Green, K. (2008). Assessing the accuracy of remotely sensed data: Principles and practices. *CRC Press.* https://doi.org/10.1201/9781420055139
2. Durako, M. J. (2007). Leaf optical properties and photosynthetic leaf absorptances in several Australian seagrasses. *Aquatic Botany, 87*(1), 83-89. https://doi.org/10.1016/j. aquabot.2007.03.005
3. Gole, S., Kuppusamy, S., Das, H., Johnson, J. A., Prabakaran, N., Prajapati, S. (2023). Spatial diversity and habitat characteristics of seagrass meadows with management recommendations in the Andaman and Nicobar Islands, India. *Frontiers in Marine Science, 10*. https://doi.org/10.3389/fmars.2023.1251887
4. Guo, Y., Cao, H., Bai, Y., Han, S., Sun, Y. (2018). Spectral–spatial hyperspectral image classification with K-nearest neighbor and guided filter. *IEEE Access, 6*, 18582–18591. https://doi.org/10.1109/access.2018.2820043
5. Ha, N. T., Pham, T. D., Manley-Harris, M., Hawes, I. (2020). A comparative assessment of ensemble-based machine learning and maximum likelihood methods for mapping seagrass using Sentinel-2 imagery in Tauranga Harbor, New Zealand. *Remote Sensing, 12*(3), 355. https://doi.org/10.3390/rs12030355
6. Hamad, I. Y., Staehr, P. A. U., Rasmussen, M. B., Sheikh, M. (2022). Drone-based characterization of seagrass habitats in the tropical waters of Zanzibar. *Remote Sensing, 14*(3), 680. https://doi.org/10.3390/rs14030680
7. Hartoni, H., Siregar, V. P., Wouthuysen, S., Agus, S. B. (2022). Karakteristik reflektansi spektral lamun menggunakan data spektrometer di perairan Kepulauan Seribu. *Jurnal Kelautan Nasional, 17*(1), 13–26. https://doi.org/10.15578/jkn.v17i1.9783
8. Hedley, J. D., Dierssen, H. M., Pérez-Castro, M. Á., Russell, B. J., Enríquez, S., Vásquez-Elizondo, R. M., Randolph, K. (2017). Remote sensing of seagrass leaf area index and species: The capability of a model inversion method assessed by sensitivity analysis and hyperspectral data of Florida Bay. *Frontiers in Marine Science, 4*. https://doi.org/10.3389/fmars.2017.00362
9. Hossain, M. S., Bujang, J. S., Zakaria, M. H., Hashim, M. (2015). The application of remote sensing to seagrass ecosystems: An overview and future research prospects. *International Journal of Remote Sensing, 36*(1), 61–114. https://doi.org/10.1080/01431161.2014.990649
10. Kaul, A., Raina, S. (2022). Support vector machine versus convolutional neural network for hyperspectral image classification: A systematic review. *Concurrency and Computation: Practice and Experience, 34*(15). https://doi.org/10.1002/cpe.6945
11. Kyriazos, T., Poga, M. (2024). Application of Machine Learning Models in Social Sciences: Managing Nonlinear Relationships. *Encyclopedia, 4*(4), 1790–1805. https://doi.org/10.3390/encyclopedia4040118
12. Kuhwald, K., Schneider von Deimling, J., Schubert, P., Oppelt, N. (2022). How can Sentinel-2 contribute to seagrass mapping in shallow, turbid Baltic Sea waters? *Remote Sensing in Ecology and Conservation, 8*(3), 346–361. https://doi.org/10.1002/rse2.246

13. Kutser, T., Hedley, J., Giardino, C., Roelfsema, C., Brando, V. E. (2020). Remote sensing of shallow waters – A 50 year retrospective and future directions. *Remote Sensing of Environment, 240*, 111619. https://doi.org/10.1016/j.rse.2019.111619
14. Lang, F., Qin, F., Yang, J., Yan, S. (2018). Superpixel segmentation of polarimetric synthetic aperture radar (SAR) images based on generalized mean shift. *Remote Sensing, 10*(10), 1592. https://doi.org/10.3390/rs10101592
15. Lee, C. B., Martin, L., Traganos, D., Antat, S., Baez, S. K., Cupidon, A.,... (2023). Mapping the national seagrass extent in Seychelles using PlanetScope NICFI data. *Remote Sensing, 15*(18), 4500. https://doi.org/10.3390/rs15184500
16. Lønborg, C., Thomasberger, A., Stæhr, P. A. U., Stockmarr, A., Sengupta, S., Rasmussen, M. L., Nielsen, L. T., Hansen, L. B., Timmermann, K. (2022). Submerged aquatic vegetation: Overview of monitoring techniques used for the identification and determination of spatial distribution in European coastal waters. *Integrated Environmental Assessment and Management, 18*(4), 892–908. https://doi.org/10.1002/ieam.4552
17. Lyons, M. B., Roelfsema, C. M., Phinn, S. R. (2020). Towards a unified approach for remote sensing of seagrass species and ecosystems. *Marine Pollution Bulletin, 160*, 111625. https://doi.org/10.1016/j.marpolbul.2020.111625
18. Marcello, J., Eugenio, F. (2022). Seagrass mapping using high resolution multispectral satellite imagery: A comparison of water column correction models. *International Journal of Applied Earth Observation and Geoinformation, 113*, 102990. https://doi.org/10.1016/j.jag.2022.102990
19. Mashoreng, S., Nafie, Y. A. L., Selamat, B., Isyrini, R., Amri, K. (2021). Changes in seagrass carbon stock: Implications of decreasing area and percentage cover of seagrass beds in Barranglompo Island, Spermonde archipelago, South Sulawesi, Indonesia. *IOP Conference Series: Earth and Environmental Science, 763*(1), 012014. https://doi.org/10.1088/1755-1315/763/1/012014
20. McKenzie, L. J., Nordlund, L. M., Jones, B. L., Cullen-Unsworth, L. C., Roelfsema, C., Unsworth, R. K. F. (2021). The global distribution of seagrass meadows. *Environmental Research Letters, 16*(7), 074041. https://doi.org/10.1088/1748-9326/ac0e2a
21. Meister, M., Qu, J. J. (2024). Quantifying seagrass density using Sentinel-2 data and machine learning. *Remote Sensing, 16*(7), 1165. https://doi.org/10.3390/rs16071165
22. Mishra, A., Apte, D. (2020). Ecological connectivity with mangroves influences tropical seagrass population longevity and meadow traits within an island ecosystem. *Marine Ecology Progress Series, 644*, 47–63. https://doi.org/10.3354/meps13349
23. Nawaz, U., Anees-Ur-Rahaman, M., Saeed, Z. (2025). A survey of deep learning approaches for the monitoring and classification of seagrass. *Ocean Science Journal, 60*(2). https://doi.org/10.1007/s12601-025-00213-1
24. Nguyen, T., Sous, D., Mengersen, K., Liquet, B. (2021). Mapping of coral reefs with multispectral satellites: A review of recent papers. *Remote Sensing, 13*(21), 4470. https://doi.org/10.3390/rs13214470
25. Nurdin, N., Alevizos, E., Syamsuddin, R., Asis, H., Zainuddin, E. N., Aris, A.,... (2023). Precision aquaculture drone mapping of the spatial distribution of Kappaphycus alvarezii biomass and carrageenan. *Remote Sensing, 15*(14), 3674. https://doi.org/10.3390/rs15143674
26. Nurdin, N., Amri, K., Mashoreng, S., Komatsu, T. (2022). Estimation of seagrass biomass by in situ measurement and remote sensing technology on small islands, Indonesia. *Ocean Science Journal, 57*(1), 118–129. https://doi.org/10.1007/s12601-022-00054-2
27. Nurdin, N., Komatsu, T., Barille, L., Akbar, M. A. S., Sawayama, S., Fitrah, M. N., Prasyad, H. (2016). Spectral classifying base on color of live corals and dead corals covered with algae. In *Proceedings of SPIE 9878, Remote Sensing of the Oceans and Inland Waters: Techniques, Applications, and Challenges, 987811*. https://doi.org/10.1117/12.2227297
28. Nurdin, N., Prasyad, H., Al, S. Q., Aries, D., Pulubuhu, T., Aris, A., Aushaf, S. T., Komatsu, T. (2023). Tracking coral loss in the Spermonde Archipelago of Indonesia: 32 years of satellite monitoring from 1990 to 2022. *International Journal of Remote Sensing, 44*(19), 6111–6141. https://doi.org/10.1080/01431161.2023.2268823
29. Pittman, S. J., Swanborn, D., Thapa, B., Roelfsema, C., Baez, S., Jensen, K. (2021). Outlining a methodological pathway to improve the global seagrass map. [*Journal Name/Publication Details Unclear from Citation*].
30. Price, D. M., Felgate, S. L., Cobb, E., Young, A., Evans, C., Brittain, H., Le Bas, T., Lichtschlag, A., Huvenne, V. A. I., Barry, C., Strong, J., Carrias, A., Sanders, R., Carpenter, S., Andrade, V. (2022). Quantifying the intra-habitat variation of seagrass beds with unoccupied aerial vehicles (UAVs). *Remote Sensing, 14*(3), 480. https://doi.org/10.3390/rs14030480
31. Roelfsema, C. M., Kovacs, E. M., Phinn, S. R. (2015). Field data sets for seagrass biophysical properties for the Eastern Banks, Moreton Bay, Australia, 2004–2014. *Scientific Data, 2*, 150044. https://doi.org/10.1038/sdata.2015.40
32. Sjafrie, N. D. M., Adi, N. S., Wicaksono, P., Sani, S. Y., Ambo-Rappe, R., Selamat, M. B., Prayudha,

B., Harahap, S. D., Yuwono, D. M., Wijaya, J., Hernawan, U. E., Hafizt, M., Salsabila, H. N., Roelfsema, C. (2025). A framework for an effective nationwide seagrass data collection: A case study for Indonesia. *Ocean & Coastal Management, 271*, 107968. https://doi.org/10.1016/j.ocecoaman.2025.107968

33. Song, J., Kim, H.-H., Seo, D.-C., Ye, J. C., Park, D.-S., Jeong, J.-H. (2020). Unsupervised denoising for satellite imagery using wavelet directional CycleGAN. *IEEE Transactions on Geoscience and Remote Sensing, 59*(8), 6823–6839. https://doi.org/10.1109/tgrs.2020.3025601
34. Traganos, D., Aggarwal, B., Poursanidis, D., Topouzelis, K., Reinartz, P. (2018). Towards global-scale seagrass mapping and monitoring using Sentinel-2 on Google Earth Engine: The case study of the Aegean and Ionian Seas. *Remote Sensing, 10*(8), 1227. https://doi.org/10.3390/rs10081227
35. Unsworth, R. K. F., McKenzie, L. J., Collier, C. J., Cullen-Unsworth, L. C., Duarte, C. M., Eklöf, J. S.,... (2021). Global challenges for seagrass conservation in the Anthropocene. *Marine Pollution Bulletin, 170*, 112608. https://doi.org/10.1016/j.marpolbul.2021.112608
36. Urbina-Barreto, I., Dutrieux, E., Mahamadaly, V., Peignon, C., Quod, J.-P., Facon, M., Penin, L., Elise, S., Bureau, S., Pinel, R., Dumas, P., Adjeroud, M., Garnier, R. (2021). Which method for which purpose? A comparison of line intercept transect and underwater photogrammetry methods for coral reef surveys. *Frontiers in Marine Science, 8*. https://doi.org/10.3389/fmars.2021.636902
37. Van Houte-Howes, K. S. S., Turner, S. J., Pilditch, C. A. (2004). Spatial differences in macroinvertebrate communities in intertidal seagrass habitats and unvegetated sediment in three New Zealand estuaries. *Estuaries, 27*(6), 945–957. https://doi.org/10.1007/bf02803421
38. Wang, M., Lian, S., Xiong, X., Yang, J., Chen, C., Shi, X. (2024). Assessing the consistency and reliability of the line intercept transect method in coral cover estimation using structure from motion photogrammetry techniques. *Geocarto International, 39*(1). https://doi.org/10.1080/10106049.2024.2322065
39. Wicaksono, P., Aryaguna, P. A., Lazuardi, W. (2019a). Benthic habitat mapping model and cross validation using machine-learning classification algorithms. *Remote Sensing, 11*(11), 1279. https://doi.org/10.3390/rs11111279
40. Wicaksono, P., Fauzan, M. A., Kumara, I. S. W., Yogyantoro, R. N., Lazuardi, W., Zhafarina, Z. (2019b). Analysis of reflectance spectra of tropical seagrass species and their value for mapping using multispectral satellite images. *International Journal of Remote Sensing, 40*(24), 9104–9127. https://doi.org/10.1080/01431161.2019.1624866
41. Wicaksono, P., Harahap, S. D., Hafizt, M., Maishella, A., Yuwono, D. M. (2023). Seagrass ecosystem biodiversity mapping in part of Rote Island using multi-generation PlanetScope. *Carbon Footprints, 2*(4), 19. https://doi.org/10.20517/cf.2023.9
42. Wicaksono, P., Kamal, M. (2017). Spectral response of healthy and damaged leaves of tropical seagrass *Enhalus acoroides, Thalassia hemprichii,* and *Cymodocea rotundata*. In *Proceedings of SPIE 10421, Remote Sensing for Agriculture, Ecosystems, and Hydrology XIX*, 104210S. https://doi.org/10.1117/12.2278027
43. Wicaksono, P., Lazuardi, W. (2018). Assessment of PlanetScope images for benthic habitat and seagrass species mapping in a complex optically shallow water environment. *International Journal of Remote Sensing, 39*(17), 5739–5765. https://doi.org/10.1080/01431161.2018.1506951
44. Wicaksono, P., Maishella, A., Lazuardi, W., Muhammad, F. H. (2022). Consistency assessment of multidate PlanetScope imagery for seagrass percent cover mapping in different seagrass meadows. *Geocarto International, 37*(26), 15161–15186. https://doi.org/10.1080/10106049.2022.2096122